Hindawi
Advances in Acoustics and Vibration
Volume 2017, Article ID 1960898, 18 pages
https://doi.org/10.1155/2017/1960898

Research Article

Vibroacoustic Analysis of a Refrigerator Freezer Cabinet Coupled with an Air Duct

Onur Çelikkan and Haluk Erol

Mechanical Engineering Faculty, Istanbul Technical University, Gumussuyu, 34439 Istanbul, Turkey

Correspondence should be addressed to Haluk Erol; erolha@itu.edu.tr

Received 29 April 2016; Revised 19 October 2016; Accepted 10 November 2016; Published 9 February 2017

Academic Editor: Sven Johansson

In this study, the vibration and acoustic interactions between the structure and the cavity inside the freezer cabinet were investigated. Thus, a set of numerical and experimental analyses were performed. In the numerical analysis, the acoustic characteristics of the freezer cavity were solved, and the mixed finite element method was then implemented to analyse the coupled behaviour of the cavity with the air duct using the Acoustic Fluid-Structure Interaction (AFSI) technique. In the experimental analyses, an acoustic modal analysis of the freezer cavity and a structural modal analysis of the air duct were performed for the validation process. A good agreement was obtained among the results. Thus, the accuracy of the numerical model was confirmed. The validated models were used for optimizing the design. To solve the noise generation mechanism inside the freezer cabinet, the noise primarily generated by the freezer fan unit was measured under normal working conditions of the refrigerator, and the resonance frequencies were obtained. This information was compared with the normal modes of the air duct, and the overlapping frequencies were identified. To reduce the interaction between the source and the structure, a few design modifications were applied to the air duct. Thus, the structural-borne noise radiating from the air duct into the freezer cavity was reduced.

1. Introduction

One modern innovation is the no-frost (or frost free) type of refrigerator, which uses an autodefrost technique that regularly defrosts the evaporator in a refrigerator or freezer. This type of refrigerator is equipped with an additional ventilation fan mounted in the air duct to circulate the cooled air and aid in the defrosting process. In this type of configuration, the fan and the compressor become a source of noise, which is the primary contributor to the overall noise level of the refrigerator, thus increasing the vibration and resulting in sound level a few decibels compared to static cooling refrigerators. Furthermore, the increasing demand for larger fresh-food storage capacities results in refrigerators with larger volumes, which need faster ventilation fans to generate larger flow rates. This high-speed rotation generates more sound energy, and this situation increases the priority of the fan among the other noise sources in the refrigerator. This case demonstrates that applying new technologies in refrigerators involves additional noise and vibration sources, which need to be investigated.

Baran et al. observed that the primary source of vibration typical for a no-frost refrigerator is the imbalance of the blades of the ventilation fan, which stimulates the plenum and effectively causes the entire structure to vibrate [1]. Seo et al. achieved a reduction in the refrigerator's sound pressure level by isolating the transmission of ventilation noise between the freezer compartment and the machinery room [2]. Takushima et al. searched for the sound sources using the sound intensity method, which indicated that the noise radiated through the openings of the front board [3]. Igarashi and Kitagawa performed CFD (Computational Fluid Dynamics) analyses by evaluating the flow fields of a propeller fan used in the freezing compartment of household refrigerators [4]. Kim et al. identified the source of excessive noise in a small fan-motor system for household refrigerators. They investigated an undesirable effect of cogging torque from the BLDC motor, which prevented the smooth rotation

of the rotor and resulted in noise [5]. Gue et al. conducted experimental and numerical investigations on the aerodynamic noise of an axial fan to develop a low noise fan, which was used to cool a compressor and a condenser in the mechanical room of a household refrigerator [6]. Öztürk and Erol showed that the contribution of structure-borne noise from the vibrating panels to the overall noise levels is significant for end users because of its relationship to noise and comfort, especially at low frequencies [7].

The goal of this study is to analyse the acoustic characteristics of the freezer compartment coupled with the air duct. Hence, the study is divided into two sections. In the first section, fluid analyses have been performed with the fan blade in the air duct, and the pressure distribution is solved in the interior surfaces of the fan louver and the evaporator cover. In the second section, coupled acoustic modal analyses have been performed between the air duct and the freezer compartment using the acoustic-structure interaction techniques. The results obtained from the numerical solutions have been validated by the experimental results. In the validation process, an experimental modal analysis was performed for the air duct, and an experimental acoustic modal analysis was performed for the freezer compartment using an external sound source. Consequently, the vibration characteristics of the air duct have been resolved, and the contribution to the noise generation in the freezer compartment has been observed.

2. Theory

For the acoustic-structure system, the structure is described by the differential equation of motion for a continuum body assuming small deformations whereas the fluid is described by the acoustic wave equation. Coupling conditions at the boundary between the structural and fluid domains ensure the continuity in displacement and pressure between the domains. The governing equations and boundary conditions, as described in detail by Carlsson [8], can be written as follows:

$$\begin{aligned}
&\text{Structure:} && \begin{cases} \tilde{\nabla}^T \sigma_S + b_S = \rho_S \dfrac{\partial^2 u_S}{\partial t^2} & @\Omega_S \\ +\text{Boundary and initial conditions} \end{cases} \\
&\text{Fluid:} && \begin{cases} \dfrac{\partial^2 p_F}{\partial^2 t} - c_0^2 \nabla^2 p_F = c_0^2 \dfrac{\partial q_F}{\partial t} & @\Omega_F \\ +\text{Boundary and initial conditions} \end{cases} \\
&\text{Coupling:} && \begin{cases} u_S = u_F & @\partial\Omega_{FS} \\ \sigma_S = -p_F & @\partial\Omega_{FS}, \end{cases}
\end{aligned} \tag{1}$$

where $\sigma_S(x, y, z, t)$ denote stresses, $b_S(x, y, z, t)$ denote body forces, ρ_S denotes dynamic density, $u_s(x, y, z, t)$ and $u_F(x, y, z, t)$ show displacements for the structural domain and fluid, separately, x, y, z denote the Cartesian coordinates, t denotes time in seconds, $p_F(x, y, z, t)$ denotes dynamic pressure, $q_F(x, y, z, t)$ denotes added fluid mass per unit volume, Ω's show domains, c_o is the speed of sound, and ∇ denotes a gradient of a variable; that is,

$$\nabla = \begin{bmatrix} \dfrac{\partial}{\partial x} & \dfrac{\partial}{\partial y} & \dfrac{\partial}{\partial z} \end{bmatrix}^T \tag{2}$$

and the differential operator $\tilde{\nabla}$ can be written as

$$\tilde{\nabla} = \begin{bmatrix} \dfrac{\partial}{\partial x} & 0 & 0 \\ 0 & \dfrac{\partial}{\partial y} & 0 \\ 0 & 0 & \dfrac{\partial}{\partial z} \\ \dfrac{\partial}{\partial y} & \dfrac{\partial}{\partial x} & 0 \\ \dfrac{\partial}{\partial z} & 0 & \dfrac{\partial}{\partial x} \\ 0 & \dfrac{\partial}{\partial z} & \dfrac{\partial}{\partial y} \end{bmatrix}. \tag{3}$$

The finite element formulation of both the continuum body and the acoustic fluid is used for modelling the fan louver and freezer cavity. The structure of interest in most acoustic-structure problems is two-dimensional and therefore often described using the plate or shell theory.

The structure is described by the equation of motion for a continuum body. The finite element formulation is derived with the assumption of a small displacement. The governing system of equations can be written as follows [9]:

$$M_S \ddot{d}_S + K_S d_S = f_F + f_b, \tag{4}$$

where

$$\begin{aligned}
M_S &= \int_{\Omega_S} N_S^T \rho_S N_S \, dV, \\
K_S &= \int_{\Omega_S} \left(\check{\nabla} N_S\right)^T D_S \check{\nabla} N_S \, dV, \\
f_F &= \int_{\partial\Omega_S} N_S^T t_S \, dS, \\
f_b &= \int_{\Omega_S} N_S^T b_S \, dV,
\end{aligned} \tag{5}$$

where N_S contains the finite element shape functions for the structural domain, $d_S(t)$ is the finite element approximation of the displacement, c_S is the nodal weight functions, t_S is the surface traction vector, and

$$D_S = \begin{bmatrix} \lambda + 2\mu & \lambda & \lambda & 0 & 0 & 0 \\ \lambda & \lambda + 2\mu & \lambda & 0 & 0 & 0 \\ \lambda & \lambda & \lambda + 2\mu & 0 & 0 & 0 \\ 0 & 0 & 0 & \mu & 0 & 0 \\ 0 & 0 & 0 & 0 & \mu & 0 \\ 0 & 0 & 0 & 0 & 0 & \mu \end{bmatrix}, \tag{6}$$

where λ and μ are the Lame coefficients expressed in the modulus of elasticity, E, the shear modulus, G, and Poisson's ratio.

In Acoustic Fluid-Structure Interaction problems, the structural dynamic equation must be considered along with the Navier-Stokes equations of fluid momentum and the flow continuity equation. The governing equations for an acoustic fluid can be derived using the following assumptions for the compressible fluid: the fluid is inviscid; the fluid only undergoes small translations; and the fluid is irrotational. Thereby, the governing equations for an acoustic fluid are the equation of motion

$$\rho_0 \frac{\partial^2 u_F(t)}{\partial t^2} + \nabla p_F(t) = 0, \tag{7}$$

the continuity equation

$$\frac{\partial \rho_F(t)}{\partial t} + \rho_0 \nabla \frac{\partial u_F(t)}{\partial t} = q_F(t), \tag{8}$$

and the constitutive equation

$$p_F(t) = c_0^2 \rho_F(t). \tag{9}$$

The system of equations for an acoustic domain becomes

$$M_F \ddot{p}_F + K_F p_F = f_q + f_s, \tag{10}$$

where

$$\begin{aligned} M_F &= \int_{\Omega_F} N_F^T N_F \, dV, \\ K_F &= c_0^2 \int_{\Omega_F} (\nabla N_F)^T \nabla N_F \, dV, \\ f_S &= c_0^2 \int_{\partial\Omega_F} N_F^T n_F^T \nabla p \, dS, \\ f_q &= c_0^2 \int_{\Omega_F} N_F^T \frac{\partial q}{\partial t} \, dV, \end{aligned} \tag{11}$$

where N_F contains the finite element shape functions for the fluid and n's denote normal vectors.

At the boundary between the structural and fluid domains, denoted as Ω_{SF}, the fluid particles and the structure move together in the normal direction of the boundary. Furthermore, the acoustic-structure problem can be described by an unsymmetrical system of equations as follows:

$$\begin{bmatrix} M_S & 0 \\ \rho_0 c_0^2 H_{SF}^T & M_F \end{bmatrix} \begin{bmatrix} \ddot{d}_S \\ \ddot{p}_F \end{bmatrix} + \begin{bmatrix} K_S & -H_{SF} \\ 0 & K_F \end{bmatrix} \begin{bmatrix} d_S \\ p_F \end{bmatrix} = \begin{bmatrix} f_b \\ f_q \end{bmatrix}, \tag{12}$$

where H_{SF} denotes spatial coupling matrix.

3. Numerical Studies

The numerical simulations were performed using the FEM solver ANSYS Workbench R15.0. In the frame of this study, each component composing the freezer compartment was first investigated individually. Thus, acoustic analyses of the freezer cavity and the modal analysis of the fan louver and evaporator cover were performed so that the mode frequencies and mode shapes could be obtained. Then, to create a realistic model, the flow field inside the air duct was modelled and included in the analyses. Lastly, a coupled modal analysis was performed to solve the problem between the structure and the acoustic cavity. The change in the acoustic modes of the freezer cavity was observed.

The fluid-structure interaction simulations were performed using the multifield solver, which used an implicit sequential coupling to calculate the interactions between the fluid and structural analyses. The FSI techniques are used to compute the effects between the acoustic and structural domains using specialized acoustic elements.

In the details of the analysis process, the state variables were defined, and the mathematical model was built to describe the physical phenomena. The mathematical model may deviate from the actual model due to various assumptions, such as viscosity and compressibility for the fluid flow and stiffness and damping for the structure.

It is widely accepted that the element size in element-based acoustic computations is related to the wavelength. In modelling, the element size has been chosen very small to ensure the sufficient number of elements per wavelength that corresponding to upper limit of frequency. The properties such as density and bulk modulus have a significant role in specifying the wavelength also defined for the fluid media. Before performing an experimental analysis to validate the numerical studies, it is possible to perform a preliminary examination basically. To show the cause of the similarity of the freezer cavity to the rectangular box, the analytical solution is also available. The equivalent box model with the same outer size could be easily used to represent the cavity model [10].

The interior of a freezer compartment resembles a closed rectangular volume, which has a simple analytical solution for its natural frequencies and acoustical modes. The natural frequencies can be calculated as follows:

$$f_{ijk} = \frac{c}{2} \sqrt{\left(\frac{i}{L_x}\right)^2 + \left(\frac{j}{L_y}\right)^2 + \left(\frac{k}{L_z}\right)^2} \,(\text{Hz}). \tag{13}$$

Furthermore, the mode shapes can be calculated as follows:

$$\Psi_{ijk} = \cos\frac{i\pi x}{L_x} \cos\frac{j\pi y}{L_y} \cos\frac{k\pi z}{L_z}, \tag{14}$$

where $L_x = 0.661$ m and is the width of the freezer cabin; $L_y = 0.447$ m and is the height of the freezer cabin measured from the bottom to the top; and $L_z = 0.446$ m and is the depth of the freezer cabin measured from the fan louver to the freezer door. The speed of sound is calculated at room temperature (at 25°C), and the indexes for the normal modes of vibration $i = 0, 1, 2, \ldots$, $j = 0, 1, 2, \ldots$, and $k = 0, 1, 2, \ldots$. Figure 1 depicts the inner dimensions of the freezer compartment and the isometric 3D model.

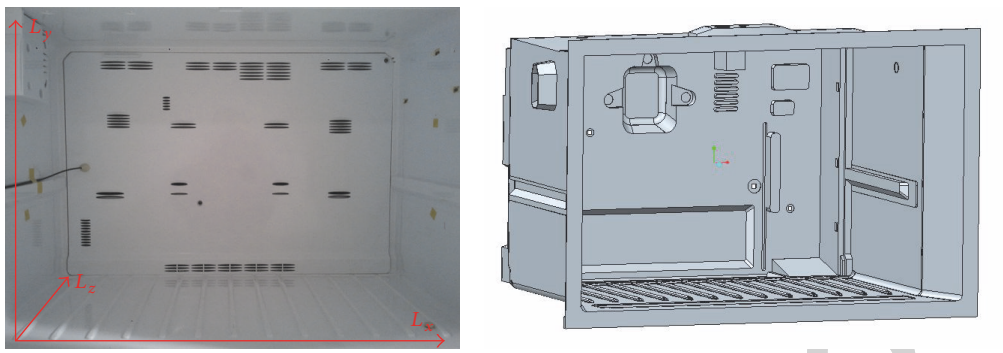

Figure 1: Inner dimensions of the freezer compartment and the isometric 3D model.

Table 1: Comparison of the analytical and numerical natural frequencies.

Mode (#)	Theory (Hz)	FE model (Hz)	Difference (%)
1	255.2	259.4	1.6
2	373.6	383.7	2.5
3	381.7	384.5	0.7
4	448.4	463.2	3.2
5	457.9	463.9	1.3
6	509.5	518.9	1.8
7	533.0	543.2	1.9
8	587.4	602.0	2.4
9	627.0	645.4	2.5
10	635.1	645.8	1.7

A convergence study has been performed on the number of elements to obtain a better accuracy between the numerical and experimental models. The convergence study can be described as follows: the acoustic modes of the cavity are computed for models with an increasing number of elements. Increasing the number of elements increases the accuracy of the model until a certain number of elements is reached; beyond this number, the accuracy does not considerably improve. A minimum number of elements should be used for a satisfactory accuracy.

To define the acoustic model in the simulation environment, the dimension of the cavity in the freezer cabin and the characteristics of the fluid (air at 25°C) were entered, and the natural frequencies and mode shapes were computed.

A comparison of the natural frequencies between the analytical solution and the numerical solution is presented in Table 1, and Figure 2 illustrates the first three numerical acoustic mode shapes of the freezer cavity.

The results obtained using the finite element model of the freezer cavity closely match those obtained analytically from the rectangular box model. In terms of the natural frequency, the largest difference occurs at 463.2 Hz, where the absolute difference is 14.8 Hz (3.2%). The primary reason for this discrepancy is the minor geometrical differences among the models. At other frequencies, the differences do not exceed the ratio of 2.5%, which indicates that the numerical model agrees extremely well with the analytical model.

Table 2: Material properties of the fan louver and the evaporator cover.

Property	Fan louver	Evaporator cover
Density (kg/m^3)	932	4660
Young modulus (Pa)	900000000	700000000
Poisson ratio	0.42	0.30

Table 3: First ten natural frequencies of the fan louver and the evaporator cover.

Mode (#)	Fan louver (Hz)	Evaporator cover (Hz)
1	4.8	15.0
2	36.5	18.3
3	49.0	35.8
4	54.6	58.8
5	76.3	73.6
6	105.1	80.5
7	111.2	90.5
8	130.6	103.5
9	132.3	110.5
10	150.2	117.0

In household refrigerators, the freezer air duct is composed of two components, fan louver and evaporator cover, as illustrated in Figure 3. The air, which is cooled by the evaporator behind the freezer compartment, is blown by the freezer fan unit and passes through the air duct to the freezer compartment. The evaporator cover has a few ribs that lead air to the openings, that is, discharge holes, located on the fan louver.

To identify the natural frequencies and mode shapes of the air duct, a three-dimensional finite element analysis and simulation were performed. In the numerical model, the evaporator cover and fan louver were modelled as coupled and flexible. Both of the components are made of polypropylene, and the material properties are listed in Table 2.

The first ten natural frequencies of the fan louver and the evaporator cover calculated from the finite element models are listed in Table 3.

The fluid field of the air cavity was extracted from the air duct, and the numerical simulation of the fluid model was

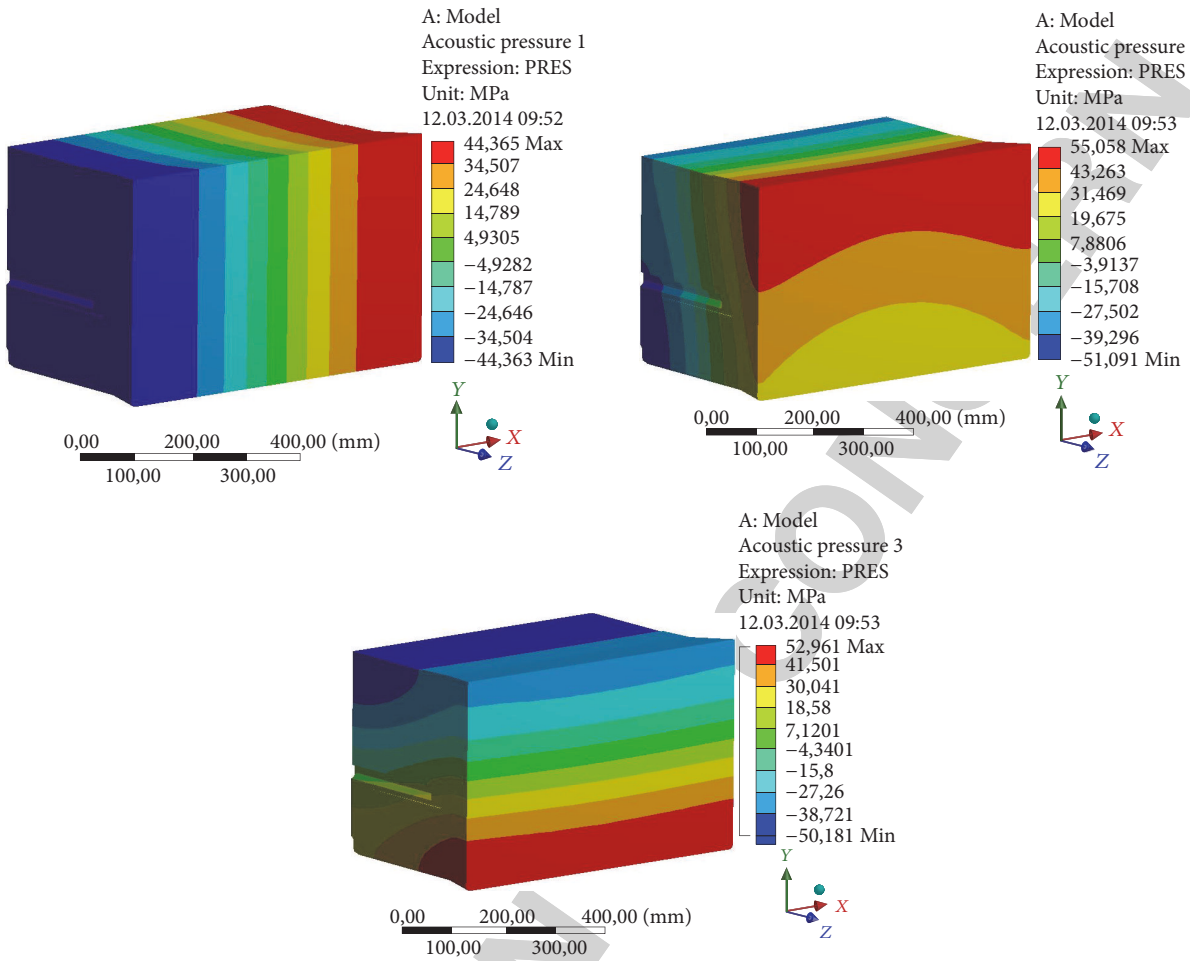

Figure 2: First three acoustic mode shapes of the freezer cavity.

Figure 3: Fan louver and evaporator cover.

created by adding the axial freezer fan driven by a motor rotating at 2200 rpm. The location of the axial fan inside the evaporator cover is depicted in Figure 4. The axial fan has 4 blades with outlet diameters of 100 mm and is located near the centre of the air inlet hole.

A no-slip boundary condition is defined at the walls, pressure inlet, and pressure outlet. The pressure inlet boundary condition is used to define the fluid pressure at the air inlet hole, and negative values are set to simulate the back pressure due to the pressure loss of the system. The pressure inlet boundary condition is applicable for both incompressible and compressible flow calculations. The pressure inlet boundary condition can be used when the inlet pressure is known and the flow rate and/or velocity are unknown.

The pressure outlet boundary conditions are defined for the discharge holes located on the fan louver. The operating pressure is set to normal working conditions, and a gauge pressure required in the pressure outlet boundary condition

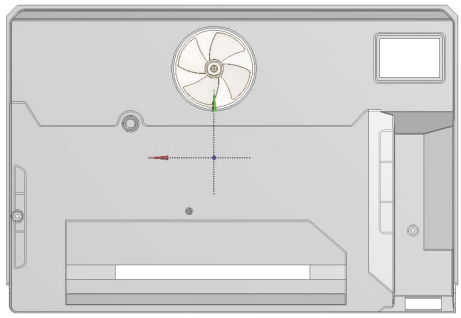

Figure 4: Location of the axial fan inside the evaporator cover.

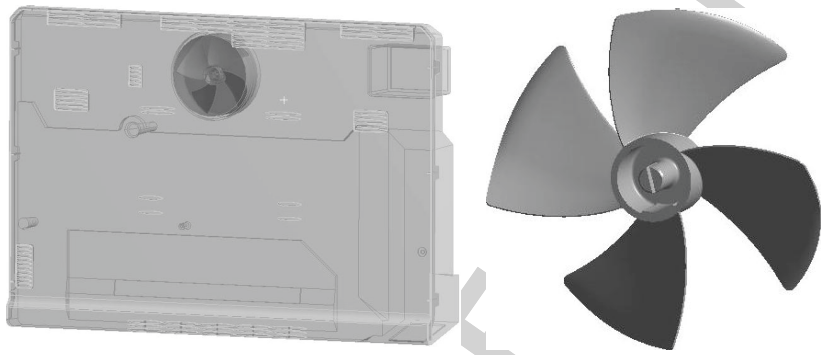

Figure 5: Isometric 3D models of the air duct cavity and the axial fan.

is specified as zero. Additionally, the backflow conditions due to the reversed flow of air across the boundary are defined. This operation minimizes the convergence errors during the iteration process. Figure 5 presents the isometric 3D models of the air duct cavity and the axial fan.

Using the finite volume method, the flow domain is discretized into approximately 2.5×10^6 control volumes. Furthermore, the inflation method is applied on all of the surfaces of the cavity to resolve the boundary layer. A flow over the propeller blades tends to cause asymmetries. To capture any possible asymmetries in the flow, the entire fan-duct geometry is simulated. A transition SST model is used to solve the flow field in the air duct. A spatial discretization is performed using the 2nd-order upwind scheme.

The transition SST model is a variant of the standard k-ω model. It combines the original Wilcox k-ω model for use near the walls and the standard k-ε model away from the walls using a blending function, and the eddy viscosity formulation is modified to consider the transport effects of the principle turbulent shear stress. This model is especially preferred for flows involving rotation, boundary layers under strong adverse pressure gradients and separation or recirculation.

In the generated model, the fluid flow conditions were supplied by the rotation of the fan blades. To simulate this motion, a "moving reference frame" technique was used. In this approach, the frame of reference is attached to the moving domain, and governing equations are modified to account for this moving frame. In fact, there is no moving part or mesh; that is, the local acceleration is added as source terms to each grid cell. This technique provides a steady approximation of the interaction between the fan and the duct.

In this study, the simulations are performed in steady-state conditions using the transition SST turbulence model. In the transition SST model, four-transport equations are solved in addition to the RANS equations. This model provides a better performance at capturing near-wall behaviour compared to the two-equation k-ε model and provides more stable solutions. This property is especially important for solving the flow field around the blades.

The pressure-based coupled solver was used as a solution method. This method provides a faster convergence compared to other methods. The computation was conducted using the second-order discretization method to obtain a higher accuracy. The calculation of the solution was obtained after 250 iterations. Figure 6 illustrates the streamlines of the velocity field in the air cavity and magnitude of the velocity at the axial fan surface.

Figure 7 depicts the pressure distributions on the front surface and the rear surface of the cavity.

The fluid-structure interaction analysis is a multiphysics problem where the interaction between two different physics phenomena, performed in separate analyses, is considered. In this study, the response of a structure under the flow-induced loads is investigated. The pressure loads obtained from the CFD analysis of the cavity are imported to the corresponding structural analysis of the fan louver. This interaction is taken at the common boundaries that the fluid domain shares with

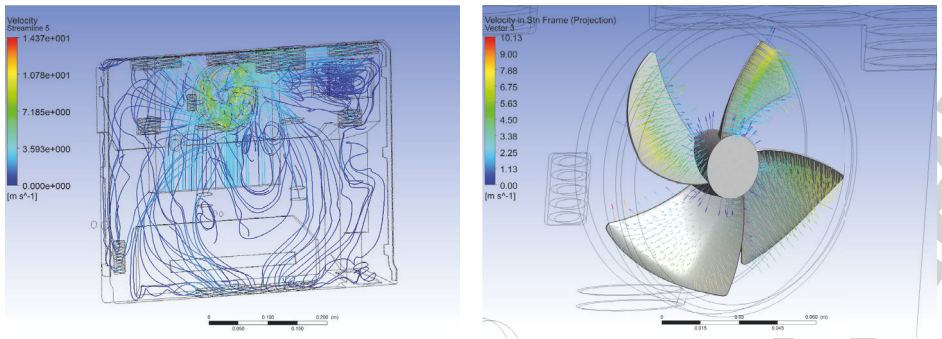

Figure 6: Streamlines of the velocity field in the air cavity and magnitude of the velocity at the axial fan surface.

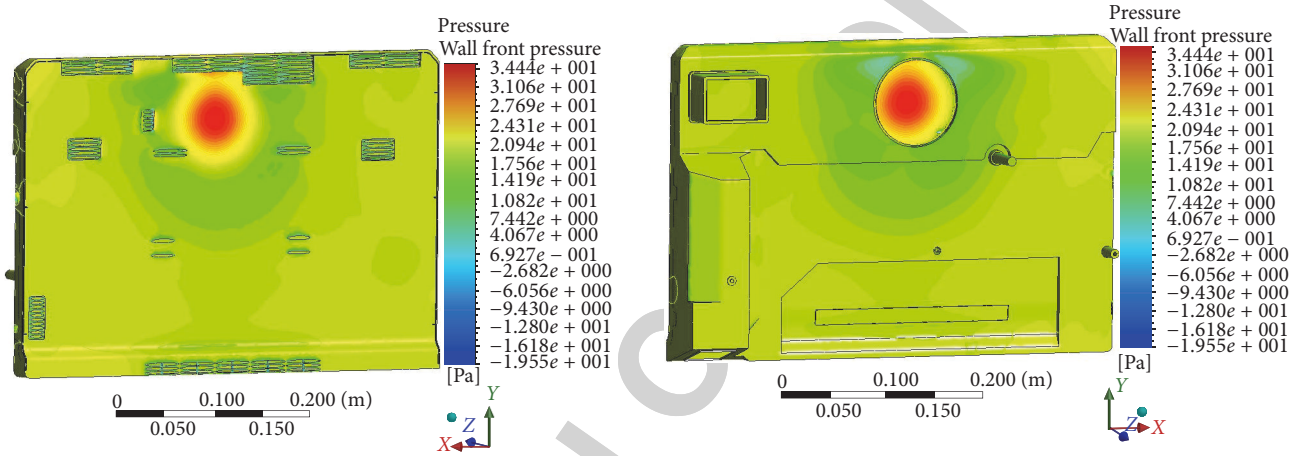

Figure 7: Pressure distributions on the front surface of the cavity and the rear surface of the cavity.

the structural domain. The results of the CFD analysis are applied to the structural analysis as an initial condition.

The partitioned approach is used for the simulation of the fluid-structure interaction. In this approach, the equations governing the flow and the displacement of the structure are solved separately with two distinct solvers. In this study, a CFD analysis is primarily performed, and the structural analysis is performed using this approach. This process indicates that the flow does not change while the structural solution is calculated. The results are interpolated to the structural analysis after the completion of the CFD analysis. In this approach, the information is exchanged at the interface between the two solvers, and this process is defined as "coupling." Figure 8 depicts the algorithm of the partitioned approach.

A one-way coupling method is performed to transfer the data from the fluid analysis to the structural analysis. In this method, the motion of a fluid flow influences a solid structure but the reaction of a solid upon a fluid is negligible. The resulting forces at the interface obtained from the fluid calculation of the cavity are interpolated to the structural mesh of the fan louver. Then, the static structural analysis is performed.

Furthermore, the fluid-structure interaction can be categorized by the degree of physical coupling between the fluid

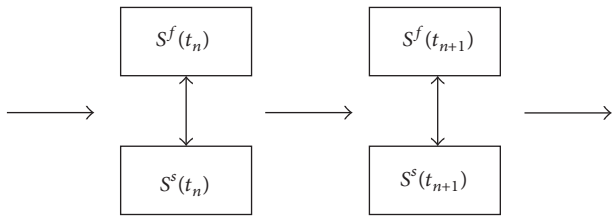

Figure 8: Algorithm of the partitioned approach.

and solid solution fields. The degree of coupling specifies how one field is sensitive to a change in the other field. Fields that are strongly coupled physically require a strong numerical coupling, and the solution is generally more difficult. In this study, the coupling degree is weak because of the physical shape of the geometries; thus, the sensitivity is less than that of strongly coupled systems.

The data transfer between the coupled participants is one of the critical parts of an FSI analysis. In our study, the static load transfer method was used in accordance with the nature of the coupling method. In the details of this data transfer method, the information is exchanged between two different types of mesh of different mediums at the interface of these mediums. This process is performed using a

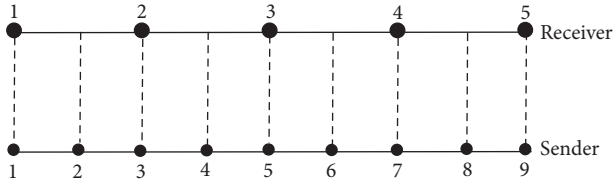

Figure 9: General grid interface.

systematic sequence. The first process of the data transfer is to match or pair the source and target mesh to generate weights. The source mesh feeds the data to the target mesh, and this matching is performed using the *General Grid Interface* mapping algorithm. The conservative nature of the *General Grid Interface* algorithm is depicted in Figure 9. This method is only available for one-way coupling.

The pressure distribution obtained from the fluid analysis on the front and back side of the air duct is transferred to the structural analysis as boundary conditions. Figure 10 depicts the importation of the pressure load to the fan louver and evaporator cover as an initial condition.

In the structural analysis of fan louver, a primary solution setup was prepared. The contact surfaces were assigned as a bond between the target surface and the body surface. As an initial condition, the fixed supports were defined at the surrounding frame of the evaporator cover to reflect the actual conditions in the freezer cabinet, and the imported pressure distribution results from the fluid analysis were applied as a load at the inner surface of the fan louver. Figure 11 depicts the contact surfaces on the fan louver and the evaporator cover.

In the analysis setting step, the "large deflection" option is set to "on." For simple linear static analyses, in which the deflection and strain are small, this option is typically set to "off" if the displacements are small enough that the resulting stiffness changes are insignificant. However, in our case, to obtain more accurate results, a prestress modal analysis will be generated in the next step, and this option must be available in this static structural analysis because the deformation in the modal analysis is high.

By setting the "large deflection" to on, the geometric nonlinearities open and consider the stiffness changes resulting from changes in the element shape and the orientation due to the large deflection, large rotation, and large strain. Therefore, these results provide more accurate solutions. However, this effect requires an iterative solution. Additionally the load needs to be applied in small increments. Thus, the solution takes a longer time. In the analysis settings, a pressure load was applied in 10 steps with a time step of 0.1 seconds between each iteration starting at time 0.

In this section, the freezer cavity has been modelled and coupled with the solved prestressed structural analysis on the fan louver. The freezer cavity was defined as an acoustic body. Air properties of the freezer cavity are listed in Table 4. The reference pressure was 20×10^{-6} N/m^2.

Table 4: Air properties of the freezer cavity.

Property	Freezer cavity
Density (kg/m^3)	1.38
Speed of sound (m/s) @25°C	346.13

Table 5: First ten natural frequencies of the freezer cavity both coupled and uncoupled with the fan louver.

Mode (#)	Uncoupled freezer cavity (Hz)	Coupled freezer cavity (Hz)
1	259.4	262.6
2	383.7	386.7
3	384.5	388.3
4	463.2	468.7
5	463.9	469.9
6	518.9	526.1
7	543.2	551.8
8	602.0	613.0
9	645.4	657.6
10	645.8	658.7

For the freezer cavity, the frequency domain acoustics can be governed by the Helmholtz equation for the acoustic pressure,, as follows:

$$\nabla \cdot \left(-\frac{1}{\rho_o}\nabla p\right) - \frac{\omega^2}{\rho_o c^2} p = 0, \quad \omega = 2\pi f. \tag{15}$$

Additionally, a coupled acoustic analysis considers the fluid-structure interaction. The governing equation for acoustics has been discretized by considering the coupling of the acoustic pressure and the structural motion at the interface. By specifying the acoustic FSI label, the structural motion and the fluid pressure are coupled at the interface. The acoustic elements used in the freezer cavity have the capabilities of translating the pressure in the nonfluid medium and the translations in the x, y, and z directions at the interface.

The dissipative effects due to the fluid viscosity and the absorption resulting from the damping are neglected. The boundaries enclosing the acoustic cavity are assumed to be hard, and the pressure gradients on all boundaries without the FSI interface are hence set to zero. Before performing the analysis, all of the openings in the fan louver were closed to fulfil the requirements of the acoustic FSI at the interface.

Table 5 lists a comparison of the first ten natural frequencies of the freezer cavity both coupled and uncoupled with the fan louver.

When the obtained results are compared, it can be clearly observed that the impact of the fan louver on the freezer cavity increases the natural frequency of the freezer cavity. These differences result in an approximate increase in the higher frequencies (2%). However, there is almost never a

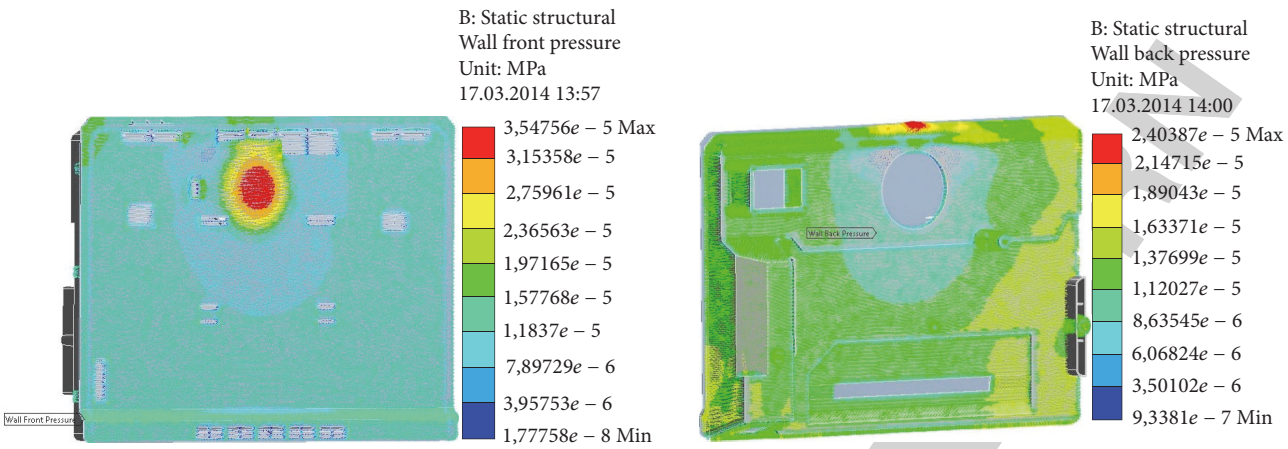

Figure 10: Pressure load imported to the fan louver and evaporator cover as an initial condition.

Figure 11: Contact surfaces on the fan louver and the evaporator cover.

change in the mode shapes of the freezer cavity in comparison to the uncoupled results of freezer cavity.

Figure 12 illustrates the first three mode shapes of the freezer cavity coupled with the fan louver calculated from the finite element model.

4. Experimental Studies

Experimental measurements were performed to validate the numerical model. Thus, the experimental acoustic modal analysis for the freezer cavity and the modal analysis for the fan louver and evaporator cover were conducted. The entire data acquisition process was achieved using a no-frost refrigerator. Figure 13 provides an image of the studied refrigerator.

The dynamic behaviour of cavity is expressed with three modal parameters; these are natural frequencies (ω_n), modal damping ratios (ζ_n), and mode shapes (Φ). The algorithm used to extract these parameters from the experimental model is based on a frequency domain curve fitting of the transfer function $H(\omega)$ between the pressure measured at point i inside the cavity and the pressure measured at point k in front of the sound source used to create the pressure field. The transfer function could be expressed in terms of the modal parameters by modal superposition as follows [10]:

$$H(\omega) = \frac{P_i}{P_k}(\omega) = \sum_{i=1}^{m} \frac{\Phi_{im}\Phi_{km}}{M_m\left(\omega_{m-}^2 \omega^2 + 2\zeta_m \omega \omega_m\right)}, \quad (16)$$

where M_m is the modal mass; ω_m is the natural frequency; ζ_m is the damping of mode m; and Φ_{im} is the modal participation of mode m at point i. The mode shapes can be expressed proportional to the modal participation as follows:

$$\begin{Bmatrix} \text{modeshape}_m(x_1) \\ \cdots \\ \text{modeshape}_m(x_k) \\ \cdots \end{Bmatrix} = \alpha_m \begin{bmatrix} \Phi_{m1}\Phi_{mk} \\ \cdots \\ \Phi_{mk}\Phi_{mk} \\ \cdots \end{bmatrix}, \quad (17)$$

where α_m is the coefficient of proportionality for the mode m. The system presented in Figure 14 is used to perform the acoustic modal analysis.

The signal from a white noise generator is limited between 0 and 1250 Hz, and an amplifier is used to adjust the level of

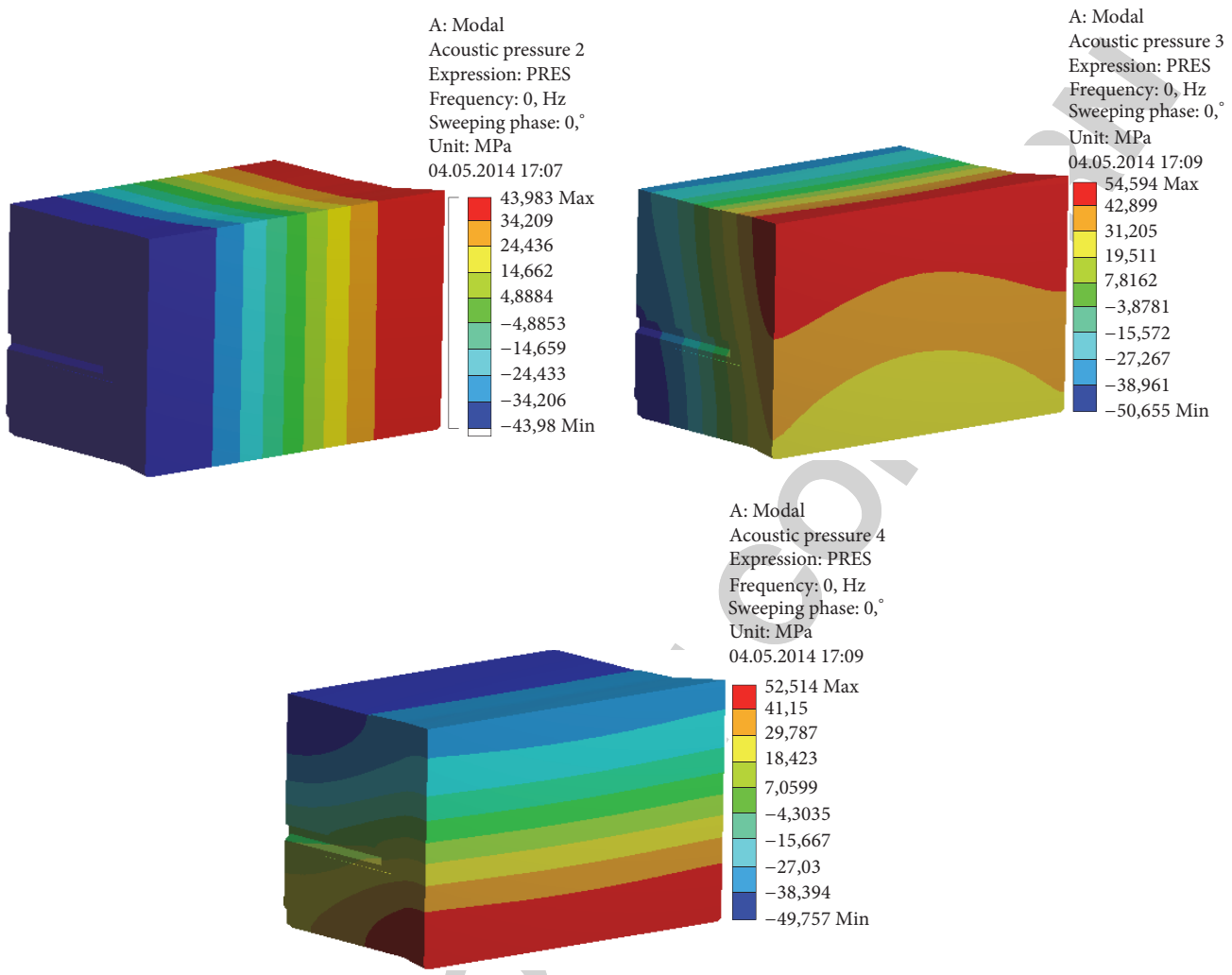

Figure 12: First three mode shapes of the freezer cavity coupled with the fan louver calculated from the finite element model.

the signal received by the loudspeaker to acoustically excite the freezer cavity. The loudspeaker was located at the location of the axial fan at the centre of the air inlet hole inside the air duct and isolated from the evaporator cover with soft foam. Figure 15 depicts the positions of the loudspeaker and the reference microphone.

Before the measurement, entire accessories, such as an ice tray and a glass shelf, were removed. The acoustic pressure measurement was performed at a total of 12 points over four rows with three different microphone positions inside the freezer cavity. Figure 16 shows the four rows of the microphone positions.

The signals were acquired using GRAS 46AE (1/2)″ free-field microphones with a 4-channel FFT analyser linked to a computer for postprocessing. Two microphones were used for one measurement: the first microphone, which was located close to the sound source, was used as a reference signal whereas the second microphone, which was located inside the freezer cavity, was used as a response signal. The acquisition processes were repeated 12 times for each measuring position. The FFT analyser computes the autospectrum of each channel as well as the cross spectrum between the reference microphone connected to channel 1 and the response microphone connected to channel 2. This information is required to calculate both the transfer function, H_1, and the coherence, ν. The frequency response function between the microphone responses at all of the grid points with respect to the reference microphone was measured (Pa/Pa)

$$H_1 = \frac{G_{xx}G_{yy}}{G_{xy}},$$
$$\nu = \frac{{G_{xy}}^2}{G_{xx}G_{yy}}. \tag{18}$$

In the measurement setup, data were collected for 10 seconds at each point by taking the linear average of the signal. The frequency resolution was set to 1,563 Hz between a frequency range of 0–1250 Hz. To satisfy the better periodicity requirement of the FFT analysis, the Hanning weighting function was used. This function minimizes the leakage error.

Figure 13: Refrigerator.

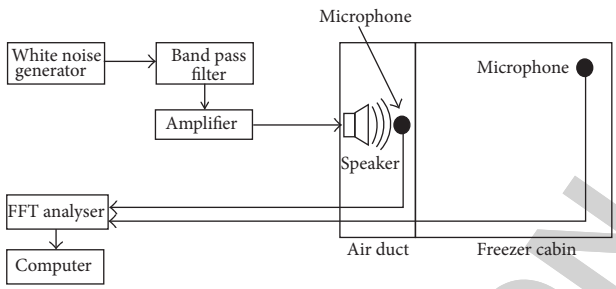

Figure 14: Acoustic modal analysis system configuration.

Table 6: First ten measured natural frequencies of the freezer cavity.

Natural frequencies (250–650 Hz) Experiment									
261.4	381.4	384.3	454.2	462.3	531.8	554.7	619.0	662.1	664.3

All of the measurements were taken at room temperature (25°C) inside the semianechoic room. Figures 17, 18, 19, and 20 illustrate the frequency response spectrum for all four measurement rows. Figure 21 shows one of the coherence functions.

From the analytical solution, we know the frequency interval that must be investigated. The analytical results indicate that the first ten modes of the freezer cavity are in a frequency range of 250–650 Hz. The first ten measured natural frequencies of the freezer cavity are presented in Table 6.

However, when the frequency response spectrum was investigated, certain peak frequencies were observed in a frequency range of 0–250 Hz. Generally, these lower peak values cannot belong to modes of the cavity because of the dimensions of the cavity. The primary reason for this phenomenon could be the structural-borne noise, which radiates from the vibration in the air duct. Thus, these lower peak frequencies are clearly observed at all of the measurement points. Hence, the dynamic behaviour of the air duct is also analysed within the scope of this study. Table 7 lists the measured peak frequencies obtained from the experiments in the range of 0–250 Hz.

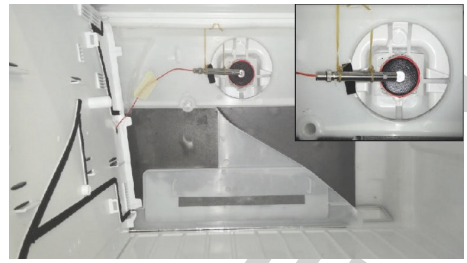

Figure 15: Position of the loudspeaker and the reference microphone.

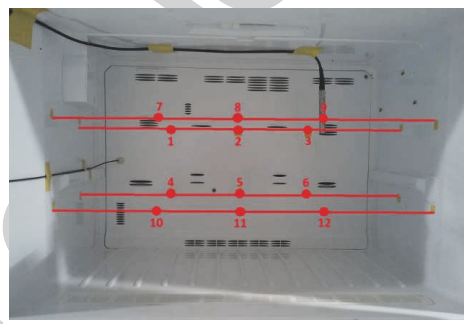

Figure 16: Four rows of the microphone positions.

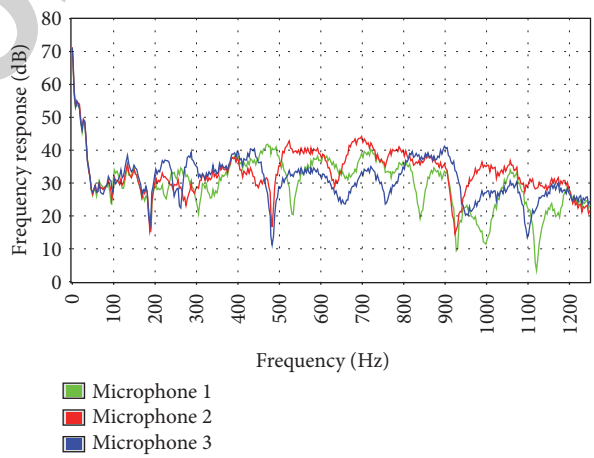

Figure 17: Frequency response spectrum (upper rear row).

Table 7: Measured peak frequencies obtained from the experiments in the range of 0–250 Hz.

Peak frequencies (0–250 Hz)									
31.2	56.2	65.6	87.5	103.1	118.7	134.3	150.0	178.1	203.1

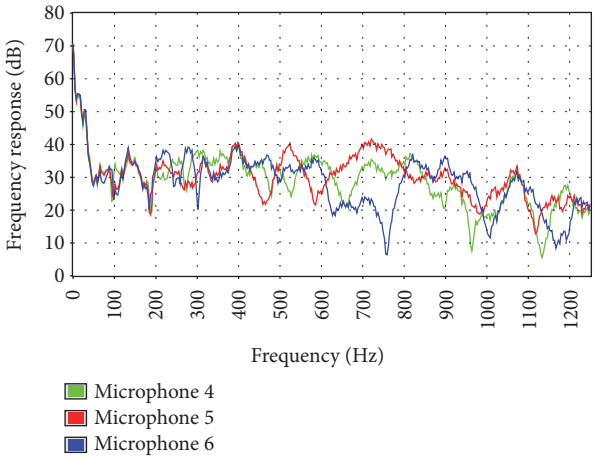

Figure 18: Frequency response spectrum (lower rear row).

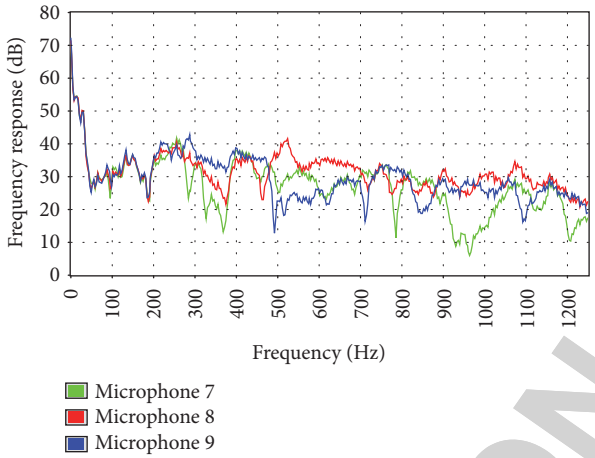

Figure 19: Frequency response spectrum (upper front row).

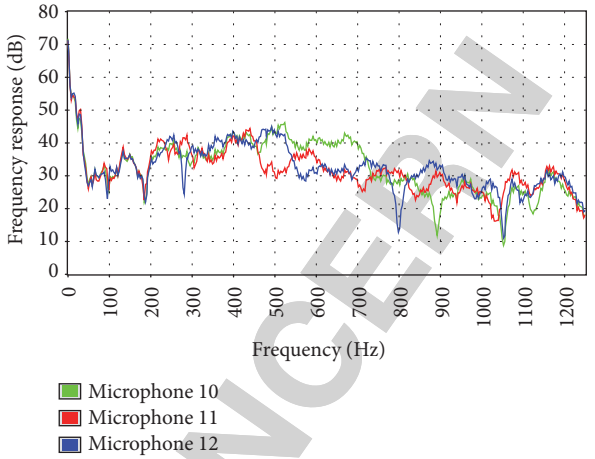

Figure 20: Frequency response spectrum (lower front row).

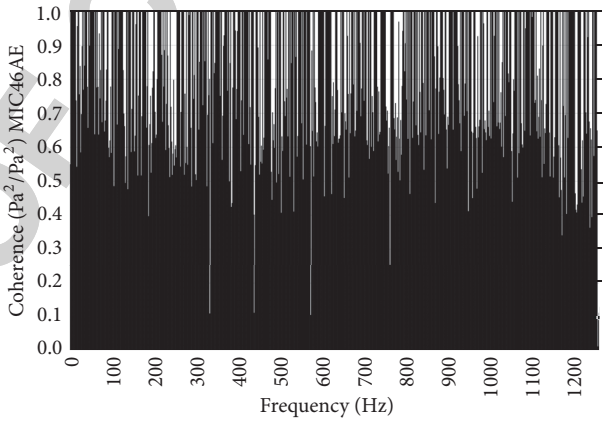

Figure 21: One of the coherence functions.

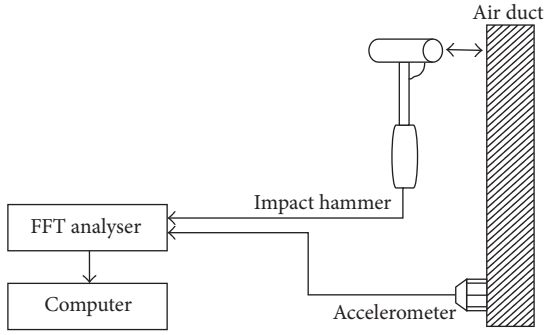

Figure 22: Modal analysis system configuration.

In the next step, the experimental modal analysis was applied to the air duct to define the dynamic characteristics of the structure under an external load. A series of frequency response functions were measured at various geometric locations using an instrumented impact hammer to supply an input force. The responses are measured in the z direction using a motion sensor, that is, an accelerometer. The system configuration presented in Figure 22 is used to perform the modal analysis.

The air duct is composed of two separate components: one is the evaporator cover and the other one is the fan louver. These two components were analysed individually. The evaporator cover and the fan louver were suspended with elastic cords from two points to simulate the free – free conditions as much as possible. The measurements were obtained from 84 points for the evaporator cover and 103 points for the fan louver. Figure 23 depicts the points on the fan louver and the evaporator cover where the measurements were obtained.

The experiment was performed with a 4-channel FFT analyser, where one channel was used to acquire the force signal and one channel was used for the acceleration signal simultaneously. The frequency response functions were measured between 0 and 250 Hz using a frequency resolution of 0.78 Hz. The excitation was provided in the horizontal direction by an impact hammer from one point, and the response was measured at all of the defined points. A rubber

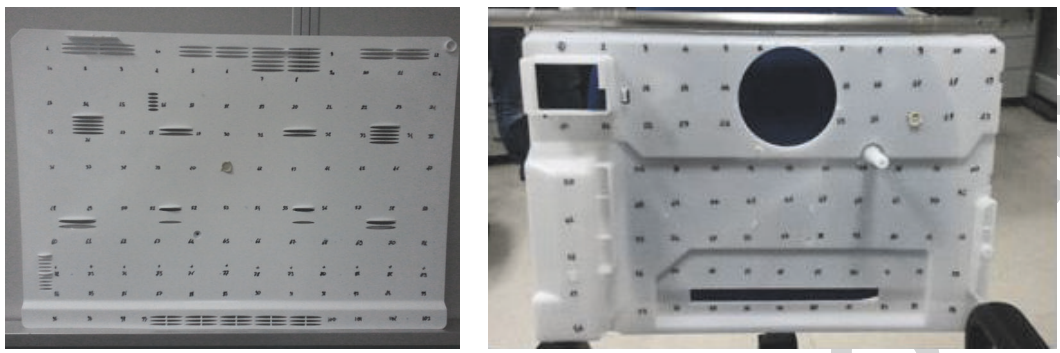

Figure 23: Measurement points on the fan louver and the evaporator cover.

Table 8: First ten experimentally measured natural frequencies and the corresponding damping ratios of the fan louver and the evaporator cover.

Natural frequencies (Hz)			
Fan louver		Evaporator cover	
Hz	%	Hz	%
5.0	2.1	14.1	2.6
37.0	2.4	18.8	1.7
46.5	1.5	32.8	3.1
55.5	2.5	56.3	2.2
77.0	0.8	70.3	2.7
104.0	1.3	79.7	1.3
112.0	2.4	89.8	3.0
129.0	4.1	101.0	3.2
133.0	2.9	107.0	1.9
149.0	3.1	114.0	3.1

tip impact hammer was used to provide a long pulse and excite a narrow frequency range.

To prevent an incorrect estimation of the amplitude and frequency due to the effects of the nonperiodic signals, the measurement period was extended, and to better satisfy the periodicity requirement of the FFT process, the Hanning time weighting function was applied. This function attempts to heavily weight the beginning and end of the sample record to zero. Table 8 presents the experimentally measured ten natural frequencies and the corresponding damping ratios of the fan louver and the evaporator cover.

When the results are investigated, a common inference can be made: the modal density is higher than 100 Hz for both structures. There are five modes for the fan louver between 100–150 Hz and three modes for the evaporator cover between 100–115 Hz. Furthermore, the modal damping ratios obtained from the curve fitting algorithm using the modal animation software ME'scope were entered in the numerical analyses.

Table 9: Comparison of the first ten natural frequencies obtained from the numerical and experimental analyses for the fan louver.

Natural frequencies (Hz)	
Numerical model	Experiment
4.8	5.0
36.5	37.0
49.0	46.5
54.6	55.5
76.3	77.0
105.1	104.0
111.2	112.0
130.6	129.0
132.3	133.0
150.2	149.0

5. Evaluation of the Results

To ensure the accuracy of the numerical model, the natural frequencies and mode shapes were compared with the measured experimental data for the validation process. In the experimental analyses, the modal animation software ME'scope was used for the visualization of the mode shapes. To solve the interaction between the air duct and the freezer cavity, the overlapping frequencies were identified, and a design optimization process was performed to change the natural frequencies of the structure; thus, the interaction between the domains was reduced. The comparison of the first ten natural frequencies obtained from the numerical and experimental analyses for the fan louver are provided in Table 9.

Figure 24 illustrates a comparison of the numerical and experimental first three mode shapes of the fan louver.

As shown in Table 9, the mode frequencies, which are acquired from the experimental analysis, agreed relatively well with the existing modes obtained from the numerical model of the fan louver. Although the polypropylene material is highly damped, the experimental mode shapes of the fan louver can be clearly observed. Particularly, in the third mode, there are a few local mode shapes that have been slightly observed. The comparison of the first ten natural frequencies

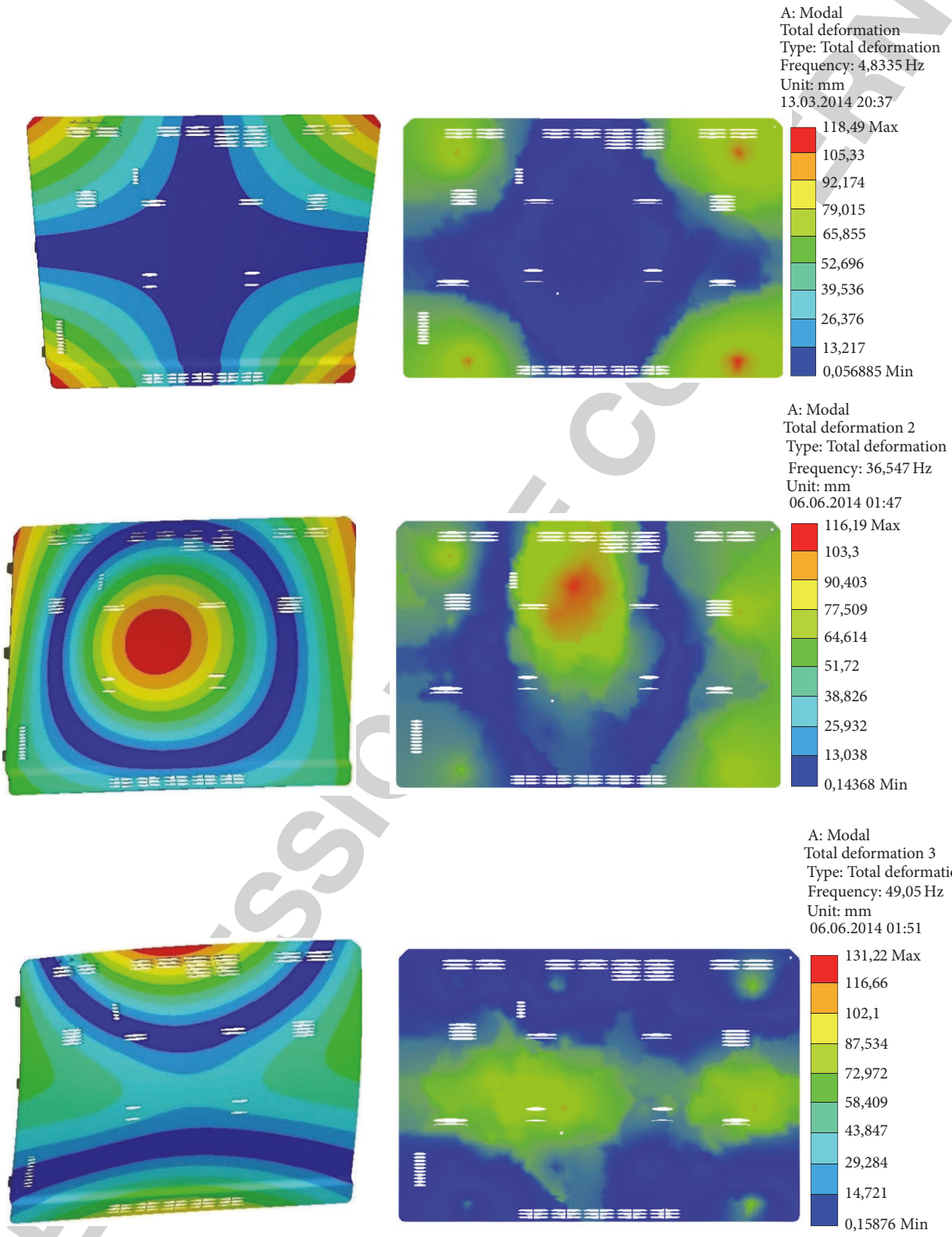

Figure 24: Numerical and experimental comparison of the first three mode shapes of the fan louver.

Table 10: Comparison of the first ten natural frequencies obtained from the numerical and experimental analyses for the evaporator cover.

Natural frequencies (Hz)	
Numerical model	Experiment
15.0	14.1
18.3	18.8
35.8	32.8
58.8	56.3
73.6	70.3
80.5	79.7
90.5	89.8
103.5	101.0
110.5	107.0
117.0	114.0

obtained from the numerical and experimental analyses for the evaporator cover is provided in Table 10.

Figure 25 presents a comparison of the numerical and experimental first three mode shapes of the evaporator cover.

In Table 10, the mode frequencies obtained from the experimental measurements are closely matched with the natural frequencies obtained from the numerical model of the evaporator cover. Despite the complexity of the geometry, the acquired data clearly reflect the motion of the structure in Figure 25. The experimental mode shapes agree with the numerical mode shapes extremely well. The numerical and experimental acoustic natural frequencies of the freezer cavity are presented in Table 11.

Between the range of 261.4 Hz and 462.3 Hz, the experimentally obtained modes are lower than the numerically obtained modes. Above this range, the experimental mode frequencies begin to diverge from the numerical mode frequencies.

Figure 26 depicts the numerical and experimental pressure distributions corresponding to the first three acoustic mode shapes of the freezer cavity.

In addition to the acquired frequency response data inside the freezer compartment, the sound pressure data were also collected under normal working conditions of the refrigerator. The measurement was performed when the freezer fun was running, and the sound pressure versus frequency spectrum data were collected by one microphone. The rotational speed of the freezer fan is 2200 rpm, and the blade passing frequency is 147 Hz for the impeller with four blades. From Figure 27, the blade passing frequency (147 Hz) and its second harmonic (294 Hz) can be easily observed.

Based on these results, if the interaction between the freezer cavity and the air duct is investigated in the range of 0–250 Hz, it can be observed that certain natural frequencies show good agreement with the peak frequencies obtained from the experimental acoustic modal analysis of the freezer cavity. Table 12 presents a comparison of the natural frequencies of the air duct and the peak frequencies of the freezer cavity.

Table 11: Comparison of the numerical and experimental acoustic natural frequencies of the freezer cavity.

Natural frequencies (Hz)	
Numerical model	Experiment
262.6	261.4
386.7	381.4
388.3	384.3
468.7	454.2
469.9	462.3
526.1	531.8
551.8	554.7
613.0	619.0
657.6	662.1
658.7	664.3

Table 12: Comparison of the natural frequencies of the air duct and the peak frequencies of the freezer cavity.

Peak frequencies (Hz)	
Freezer cavity	Air duct
31.2	32.8 (evap. cover)
56.2	55.5 (fan louver)
65.6	—
87.5	89.8 (evap. cover)
103.1	104.0 (fan louver)
118.7	—
134.3	133.0 (fan louver)
150.0	149.0 (fan louver)
178.1	—
203.1	—

In conclusion, the blade passing frequency of the freezer fan and the 10th normal mode of the fan louver are extremely close to each other. This situation indicates that the freezer fan could excite the fan louver in its nominal working frequency and cause the vibration of the fan louver. These vibrations turn into sound energy, which radiates from the fan louver and increases the amplitude of the sound pressure inside the cavity. In fact, this phenomenon occurs because one of the resonance frequencies observed in the cavity is 150 Hz. To reduce this interaction between the structure and the cavity, two methods could be used: one is decreasing the amplitude of the resonance frequency while the other is shifting the resonance frequency. The first method could be achieved by adding the damping material to the points that have a maximum deformation based on the mode shape of the fan louver at the resonance frequency. However, this method is not applicable due to the restrictions related to human health.

The technique that shifts the resonance frequency could be successful through certain design modifications. Thus, the rotation speed and the number of blades of the fan could be changed to alter the excitation frequency. However, all of these options also change the cooling performance of the refrigerator; hence, this is not a preferred method.

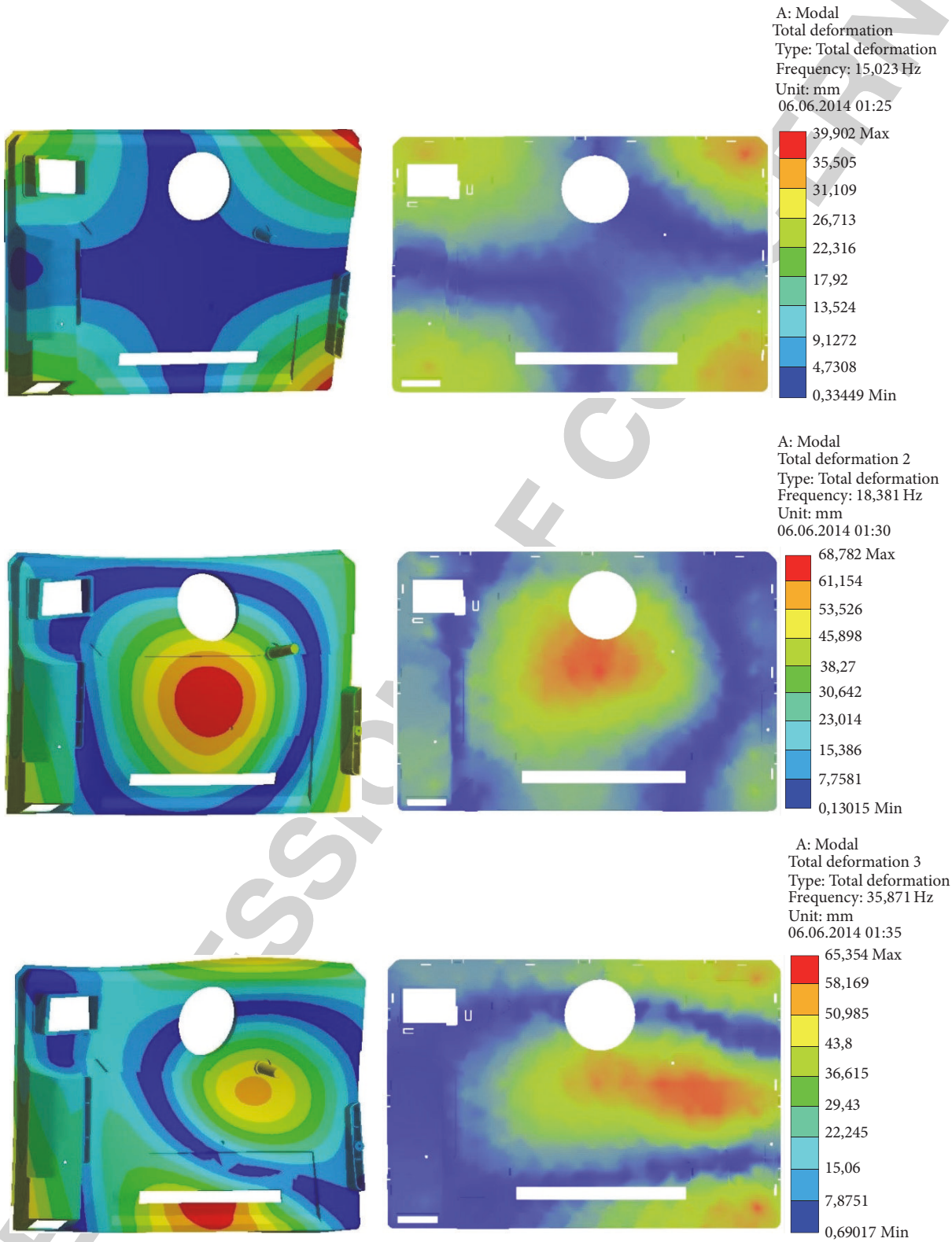

Figure 25: Comparison of the numerical and experimental first three mode shapes of the evaporator cover.

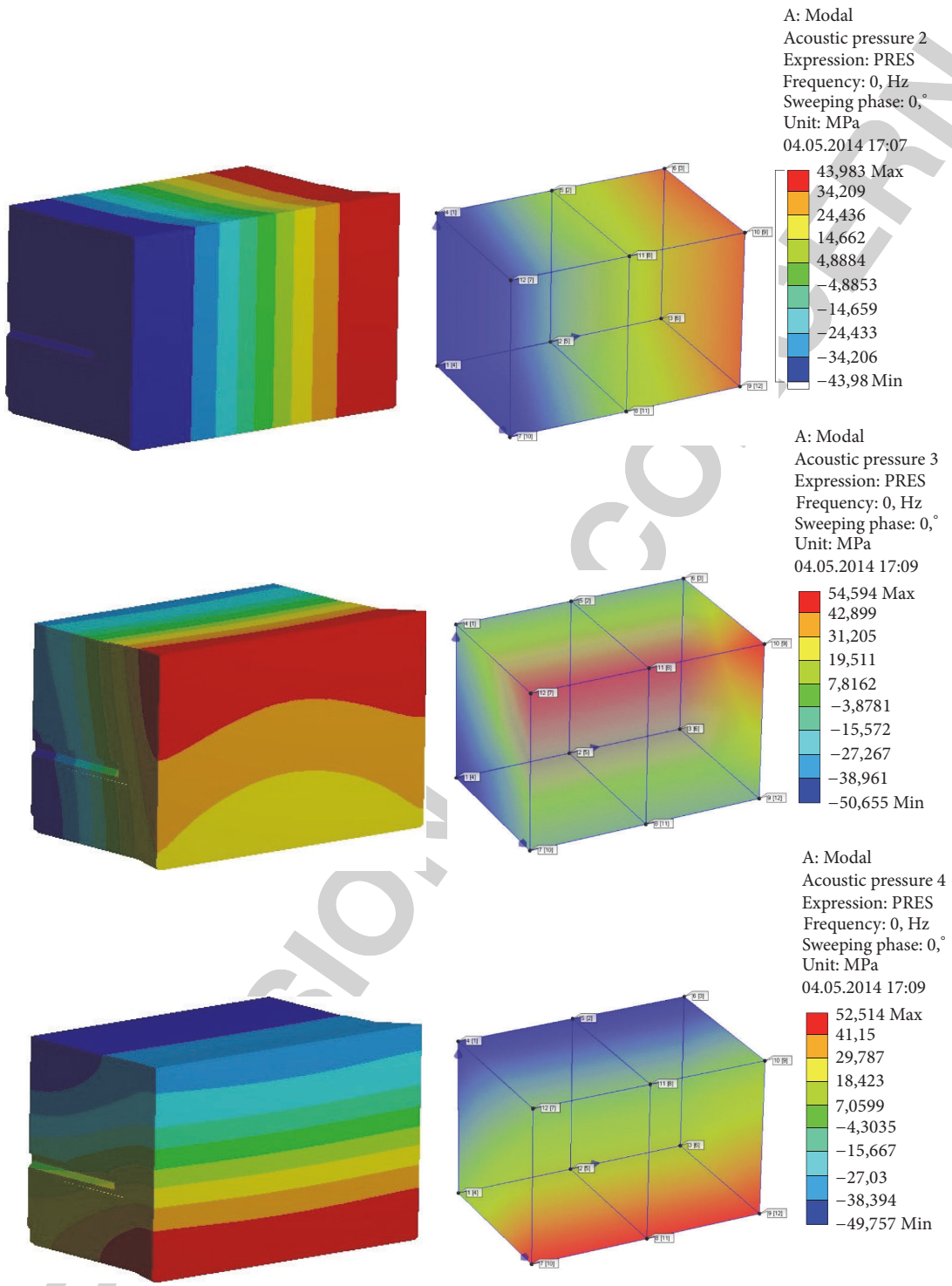

Figure 26: Numerical and experimental pressure distributions corresponding to the first three acoustic mode shapes of the freezer cavity.

In this study, the structural modification was applied to the fan louver because the other methods are not applicable to the refrigerator in reality. The thickness of the fan louver was increased to shift its natural frequencies. A change in frequencies was observed when the thickness was increased. The optimum thickness was determined as 2.1 mm (the current thickness is 2.0 mm). Table 13 presents the natural frequencies of the modified fan louver.

Using this modification, the 10th normal mode of the fan louver moved to 157.7 Hz in the frequency domain, and none

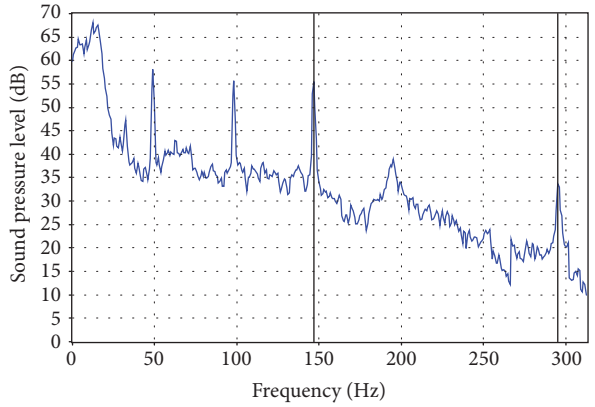

Figure 27: Frequency spectrum of the sound pressure level.

Table 13: Natural frequencies of the modified fan louver.

Natural frequencies (Hz)									
Numerical model									
5.0	38.3	51.4	57.3	80.1	110.3	116.8	137.1	138.9	157.7

of the submodes overlapped with the blade passing frequency. Thus, the interaction between the structure and the cavity was reduced.

6. Conclusions

In this study, the acoustic characteristics of the refrigerator freezer compartment are investigated. A reliable and accurate numeric model is developed to simulate the coupled behaviour of the structure and the acoustic cavity for the freezer compartment. A mixed finite element method is used to solve the acoustic-structure interaction of the acoustic cavity coupled with the elastic body. The numerical results indicate how the coupled structures change the natural frequencies and the mode shapes of the acoustic cavity.

The numeric results are validated with the experimental analyses. Thus, an experimental modal analysis of the fan louver and the evaporator cover is performed, and the natural frequencies are found. Lastly, an experimental acoustic modal analysis is implemented to the freezer cavity; thus, the normal modes that belong to both the acoustic cavity and coupled structures are obtained.

These results demonstrate that the normal modes of the fan louver and the evaporator cover change the acoustic characteristic of the freezer compartment, especially in low frequency ranges.

Lastly, the noise generation mechanism inside the freezer compartment is investigated under normal working conditions of the refrigerator. The resonance frequencies generated by the fan unit are obtained. The overlapping frequencies between the source and the structures are shifted using certain design modifications. Thus, the structural-borne noise, which radiates from the air duct into the freezer cavity, is reduced.

Competing Interests

The authors declare that they have no competing interests.

References

[1] M. Baran, R. Bolejko, P. Pruchnicki, B. Zoltogorski, and A. Dobrucki, "Refrigerator noise and vibration control and optimization," in *Proceedings of the 16th International Congress on Sound and Vibration*, Krakow, Poland, July 2009.

[2] S. Seo, T. Kwak, C. Kim, J. Park, and K. Jo, "Noise and vibration reduction of a household refrigerator," in *Proceedings of the HVAC Refrigeration Engineering*, pp. 1133–1140, 2000.

[3] A. Takushima, Y. Shinobu, S. Tanaka, M. Eguchi, and K. Matsuki, "Fan noise reduction of household refrigerator," *IEEE Transactions on Industry Applications*, vol. 28, no. 2, pp. 287–292, 1992.

[4] S. Igarashi and K. Kitagawa, "Numerical analysis for propeller fan in freezing compartment of household refrigerator," in *Proceedings of the 9th of International Symposium on Transport Phenomena and Dynamics of Rotating Machinery*, Honolulu, Hawaii, February 2002.

[5] Y.-H. Kim, B.-S. Yang, and C.-J. Kim, "Noise source identification of small fan-BLDC motor system for refrigerators," *International Journal of Rotating Machinery*, vol. 2006, Article ID 63214, 7 pages, 2006.

[6] F. Gue, C. Cheong, and T. Kim, "Development of low-noise axial cooling fans in a household refrigerator," *Journal of Mechanical Science and Technology*, vol. 25, no. 12, pp. 2995–3004, 2011.

[7] S. Öztürk and H. Erol, "Numerical and experimental studies on the structure-borne noise control on a residential kitchen hood," *International Journal of Acoustics and Vibrations*, vol. 18, no. 1, pp. 3–6, 2013.

[8] H. Carlsson, *Finite Element Analysis of Structure-Acoustic Systems; Formulations and Solution Strategies*, TVSM 1005, Structural Mechanics, LTH, Lund University, Lund, Sweden, 1992.

[9] N. Ottosen and H. Peterson, *Introduction to the Finite Element Method*, Prentice Hall, New York, NY, USA, 1992.

[10] J. C. Couche, *Active control of automobile cabin noise with conventional and advanced speakers [M.S. thesis]*, Virginia Polytechnic Institute and State University, 1999.